Coupling parameters of many-body interactions for the Al(100) surface state: A high-resolution angle-resolved photoemission spectroscopy study

J. Jiang,[1] K. Shimada,[2,*] H. Hayashi,[1] H. Iwasawa,[2] Y. Aiura,[3] H. Namatame,[2] and M. Taniguchi[1,2]

[1]*Graduate School of Science, Hiroshima University, Kagamiyama 1-3-1, Higashi-Hiroshima 739-8526, Japan*

[2]*Hiroshima Synchrotron Radiation Center, Hiroshima University, Kagamiyama 2-313, Higashi-Hiroshima 739-0046, Japan*

[3]*National Institute of Advanced Industrial Science and Technology, Tsukuba, Ibaraki 305-8568, Japan*

(Received 18 August 2011; published 17 October 2011)

We examined the dimensionless coupling parameters of many-body interactions for a free-electron-like surface-derived state in Al(100) by means of high-resolution angle-resolved photoemission spectroscopy. A kink structure was found to exist in the energy-band dispersion near the Fermi level (E_F), which was attributed to the electron-phonon interaction. At 50 K, the coupling parameters of the electron-phonon and electron-electron interactions were estimated as $\lambda_{ep} = 0.67 \pm 0.05$ and $\lambda_{ee} \sim 0.003$, respectively, indicating that the effective mass enhancement was mainly derived from the electron-phonon interaction. The temperature dependence of the kink structure, as measured by $\lambda_{ep}(T)$, was consistent with a theoretical calculation based on the Eliashberg function. A quasiparticle peak with a width of 15–20 meV was found near E_F, which was explained well by the simulated spectral function incorporating the self-energy evaluated in this study. We found that the electrons at the surface were strongly scattered by the defects at the surface and that the linewidth was significantly broadened ($\Gamma_0 = 0.238 \pm 0.006$ eV).

DOI: 10.1103/PhysRevB.84.155124 PACS number(s): 75.30.Ds, 73.20.At, 75.50.Bb, 79.60.−i

I. INTRODUCTION

Recently, the energy and momentum resolutions of angle-resolved photoemission spectroscopy (ARPES) have been drastically improved,[1–4] and it is now possible to examine fine electronic structures, such as a kink structure in the energy-band dispersion or a sudden reduction of the Fermi velocity near the Fermi level (E_F) in detail.[1–4] By means of quantitative analyses of high-resolution ARPES line shapes, one can evaluate the dimensionless coupling parameters of the electron-phonon interaction (λ_{ep}) and electron-electron interaction (λ_{ee}) at a given point on Fermi surfaces.[1–4] These parameters are important since the effective mass is given by $m^* = (1 + \lambda_{ep} + \lambda_{ee})m_b$, where m_b is the band mass. Furthermore, the superconducting transition temperature can be approximately given by $T_c = \frac{\Theta_D}{1.45}\exp[-\frac{1.04(1+\lambda_{ep})}{\lambda_{ep}-\mu^*(1+0.62\lambda_{ep})}]$,[5] where Θ_D is the Debye temperature and μ^* is the empirical value for the Coulomb coupling constant.

Aluminum (Al) is a typical trivalent metal and a superconductor with a transition temperature of 1.18 K.[6,7] The bulk-derived Fermi surface was studied by de Haas–van Alphen effect measurements,[8] and the energy-band dispersions were clarified in detail by ARPES.[9] The bulk-derived electronic states of Al are well understood based on the trivalent nearly-free-electron model.[7] The superconductivity of Al is most successfully explained by BCS theory,[10] in which the s-wave Cooper pair is formed by the electron-phonon interaction.

On the Al(100) surface, there exists a free-electron-like surface-derived state centered at the $\overline{\Gamma}$ point of the surface Brillouin zone (SBZ).[9,11–16] Similar surface states have been observed in many other systems, such as the (111) surface of noble metals,[17,18] Ni(111),[19–21] and Be(0001).[22,23] The energy distribution curves (EDCs) of the Al(100) surface state have been quantitatively examined using a one-step-model calculation.[24–26]

In this study, we determine λ_{ep} and λ_{ee} for the Al(100) surface state by means of high-resolution temperature-dependent ARPES. Many high-T_c superconductors have a low-dimensional electronic structure.[27] We believe that a detailed quantitative examination of the many-body interactions in an ideal two-dimensional Fermi liquid like the Al(100) surface state should provide a good reference for understanding the unusual physical properties of novel materials.

There are two methods of evaluating λ_{ep} based on the ARPES spectra.[28] The most widely used method is based on the temperature dependence of the ARPES linewidth, assuming the following formula:[29]

$$\Gamma_{ep}(\omega = 0, T) = 2\pi\lambda_{ep}k_BT \quad (T \gg \Theta_D), \tag{1}$$

where $\Gamma_{ep}(\omega = 0, T)$ is the ARPES linewidth at E_F ($\omega = 0$) and Θ_D is the Debye temperature. The coupling parameter can be obtained by the gradient of the ARPES linewidth, $\lambda_{ep} = \partial\Gamma_{ep}/\partial T$. Note that the lifetime broadening is related to the imaginary part of the self-energy due to the electron-phonon interaction as $\Gamma_{ep}(\omega = 0, T) = 2|\mathrm{Im}\Sigma_{ep}(\omega = 0, T)|$. By measuring the ARPES linewidth for a wide temperature range, one can evaluate λ_{ep} based on Eq. (1). However, temperature-induced defects may significantly enhance the linewidth, leading to an overestimated coupling parameter.[30–34]

The other method is to measure the kink structure in the energy-band dispersion derived from the electron-phonon interaction. The coupling parameter is evaluated by[29]

$$\lambda_{ep}(T) = -\left.\frac{\partial \mathrm{Re}\Sigma_{ep}(\omega, T)}{\partial\omega}\right|_{\omega=0}, \tag{2}$$

where $\mathrm{Re}\Sigma_{ep}(\omega, T)$ is the real part of the self-energy. The real part of the self-energy is obtained from the energy shift from the noninteracting band (ω_k^0): $\mathrm{Re}\Sigma_{ep}(\omega, T) = \omega - \omega_k^0$. Note that, due to the temperature dependence of $\mathrm{Re}\Sigma_{ep}(\omega, T)$, the magnitude of the kink structure as measured by $\lambda_{ep}(T)$ is also temperature dependent.[29] The temperature dependence of $\lambda_{ep}(T)$, however, has not been experimentally elucidated so far to the best of our knowledge.

In the case of the Shockely state in Cu(111), $\lambda_{ep} \sim 0.14$ (Refs. 35 and 36) and 0.16 (Ref. 37) have been obtained based on Eq. (1), which have reasonable agreement with $\lambda_{ep} \sim 0.14$ (Ref. 38) evaluated based on Eq. (2). For the Al(100) surface state at the $\overline{\Gamma}$ point, by contrast, the λ_{ep} value obtained from Eq. (1) is as high as $\sim$1.8.[30] It has been claimed that the temperature-induced lattice defects should cause additional linewidth broadening at elevated temperatures, giving a much higher λ_{ep}.[30,32]

Therefore, high-resolution ARPES is needed to observe the kink structure and evaluate λ_{ep} based on Eq. (2). We have conducted a high-resolution ARPES study on this surface state and have evaluated the electron-phonon coupling parameter based on the kink structure at low temperature using the photon energy of $h\nu = 43$ eV.[39] Our preliminary evaluation gave $\lambda_{ep} = 0.67$ at 30 K,[39] which was enhanced by 50% from the bulk value $\lambda_{ep} = 0.43$.[6] However, it was much smaller than the $\lambda_{ep} \sim 1.8$ (Ref. 30) evaluated from the temperature dependence of the linewidth.

In this study, we have extensively performed high-resolution temperature-dependent ARPES measurements and examined the many-body interactions in the Al(100) surface state in more detail. We described the experimental self-energy, the temperature dependence of the kink structure, and the observed narrow peak in the EDCs near E_F using theoretical Eliashberg functions.[40,41]

II. EXPERIMENT

Single-crystal Al(100) (purity 99.9999%) was cleaned by repeated cycles of Ar^+ sputtering and annealing in an ultrahigh-vacuum chamber. To remove the thick oxide layers, the first Ar^+ sputtering (at 4.5 keV) lasted for more than 10 h, followed by subsequent annealing at 400 °C for 30 min. During the experiments, a clean sample surface was prepared every 12 h by 2-h Ar^+ sputtering (4 keV) and annealing at 400 °C for 10 min. The level of impurities, such as C, O, and S, on the surface was below the detection limit of Auger electron spectroscopy. Sharp 1×1 low-energy electron-diffraction spots exhibited long-range order and an atomically clean sample surface. We also verified the absence of contaminants on the surface by angle-integrated photoemission spectra in a wide binding energy range taken at $h\nu = 330$ eV before and after the ARPES measurements.

High-resolution ARPES experiments were performed on the linear undulator beamline (BL-1) of a compact electron-storage ring (HiSOR) at Hiroshima University.[42] The present data were obtained using an angular mode of the hemispherical electron-energy analyzer (R4000, VG-Scienta, Japan). The total energy resolution was set at $\Delta E = 15$ meV for high-resolution measurements at $h\nu = 46$ eV and at 25 meV for the Fermi surface mapping at $h\nu = 76$ eV. The angular resolution was $\Delta\theta = 0.3°$, giving momentum resolutions of $\Delta k_\parallel = 0.017$ Å^{-1} at $h\nu = 46$ eV and 0.023 Å^{-1} at $h\nu = 76$ eV.

We assumed an inner potential of $V_0 = 11.2$ eV.[16] Although the electronic states localized at the surface do not have $k_\perp$ dispersion, the inner potential is useful to estimate the position of the bulk-derived electronic states. Note that the Al(100) surface state enters the bulk-band projection near E_F and becomes a resonance state.[41] To measure the surface state at its maximum intensity and away from the bulk-derived spectral features, we optimized the photon energy. We found that the photon energy $h\nu = 46$ eV was most suitable for the detailed ARPES line shape analyses.

The sample was mounted on a liquid-He-flow-type five-axis goniometer (i-GONIO LT, R-dec Co., Japan[43]) installed in the ARPES measurement chamber. By changing the azimuth and polar angles of the goniometer, we performed two-dimensional Fermi surface mapping. The sample temperatures were set at $T = 10, 50, 100, 150, 300$ K.

The pressure of the measurement chamber was below 6×10^{-9} Pa during the measurements.

III. SELF-ENERGY ANALYSIS

The ARPES spectral features are given by the single-particle spectral function $A(k,\omega)$. As we are examining an isotropic two-dimensional electron system near E_F, we assume that the k dependence of the self-energy can be neglected, namely, $\Sigma(k,\omega) \sim \Sigma(\omega)$. In this case, the spectral function is given by

$$A(k,\omega) = -\frac{1}{\pi}\frac{\mathrm{Im}\Sigma(\omega)}{\left[\omega - \omega_k^0 - \mathrm{Re}\Sigma(\omega)\right]^2 + [\mathrm{Im}\Sigma(\omega)]^2}, \quad (3)$$

where ω_k^0 represents the energy of the noninteracting band.[3,4,23,44]

In the case that the electron-scattering processes derived from the electron-phonon and electron-electron interactions can be regarded as independent, the lifetime broadening of a quasiparticle is given by $\Gamma = 2|\mathrm{Im}\Sigma| = \Gamma_0 + \Gamma_{ep} + \Gamma_{ee}$, where Γ_{ep} and Γ_{ee} are the lifetime broadening due to the electron-phonon and electron-electron interactions, respectively. The $\Gamma_{ep} + \Gamma_{ee}$ term gives the energy-dependent linewidth broadening. The Γ_0 term, on the other hand, is an energy-independent term that should be derived from the electron-defect interaction in the case of the Al(100) surface state, as described below.

If $\mathrm{Im}\Sigma(\omega)$ is given, $\mathrm{Re}\Sigma(\omega)$ can be calculated using the Kramers-Kronig transform,

$$\mathrm{Re}\Sigma(\omega) = \frac{1}{\pi}\mathrm{P}\int_{-\infty}^{+\infty}\frac{\mathrm{Im}\Sigma(\omega')}{\omega' - \omega}d\omega'. \quad (4)$$

To experimentally determine the self-energy in this study, we analyzed the line shape of the momentum distribution curve (MDC). The MDC width (δk) is related to $\mathrm{Im}\Sigma(\omega)$ by $\Gamma = 2|\mathrm{Im}\Sigma(\omega)| = \delta\omega = (\partial\omega/\partial k)\delta k$, where $(\partial\omega/\partial k)$ is the gradient of the energy band. The MDC peak position at a given ω gives an energy-band dispersion. To evaluate $\mathrm{Re}\Sigma_{ep}$, we assumed the noninteracting band to be $\omega_k^0 = -\omega_0^* + (\omega_0^*/k_F^2)k_\parallel^2$, which was determined by the fit of observed band points in a wide energy range.

IV. RESULTS AND DISCUSSION

A. Fermi surface mapping and band dispersion

Figure 1 shows the observed Fermi surface of the Al(100) surface state taken at $h\nu = 76$ eV and $T = 10$ K. The dashed lines indicate the boundary of the SBZ of the fcc (100) surface.[44] A circular surface-derived Fermi surface centered at

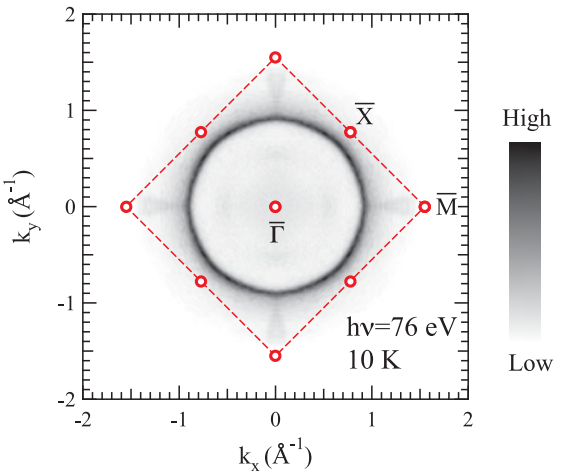

FIG. 1. (Color online) The observed Fermi surface of the Al(100) surface state, taken at $h\nu = 76$ eV and 10 K. The dashed lines indicate the SBZ of the fcc (100) surface.

the $\overline{\Gamma}$ point of the first SBZ can clearly be seen. The observed Fermi surfaces taken at $h\nu = 76$ and 143 eV (not shown) were identical to that in our previous study taken at $h\nu = 167$ eV,[39] which was consistent with the two-dimensional nature of the surface state.

Figure 2(a) shows the ARPES intensity plot of the Al(100) surface state along the $\overline{\Gamma M}$ direction measured at $h\nu = 46$ eV and $T = 10$ K, exhibiting a parabolic dispersion. By fitting the MDC and EDC to a Lorentzian on a linear background, we evaluated the peak positions in Fig. 2 (b). Using the evaluated band points, we determined the parabolic dispersion $\omega_k = -\omega_0^* + (\omega_0^*/k_F^2)k_\parallel^2$, where $\omega_0^* = 2.81 \pm 0.03$ eV and the Fermi wave number $(k_F) = 0.907 \pm 0.005$ Å^{-1}. The obtained band-bottom energy agrees reasonably well with the various theoretical calculations [$\omega_0 = 2.62$ (Ref. 26), 2.65 (Ref. 45), and 2.86 eV (Ref. 41)]. The band mass of the surface state was estimated to be $m_b = \hbar^2/(\partial^2\omega_k^0/\partial k^2) = (1.02 \pm 0.02) \times 10^{-30}$ kg $= (1.12 \pm 0.02)m_e$, where m_e is the electron mass. It is consistent with the previously determined values $m_b = 1.18m_e$ (Ref. 9) and $1.27m_e$ (Ref. 39). The

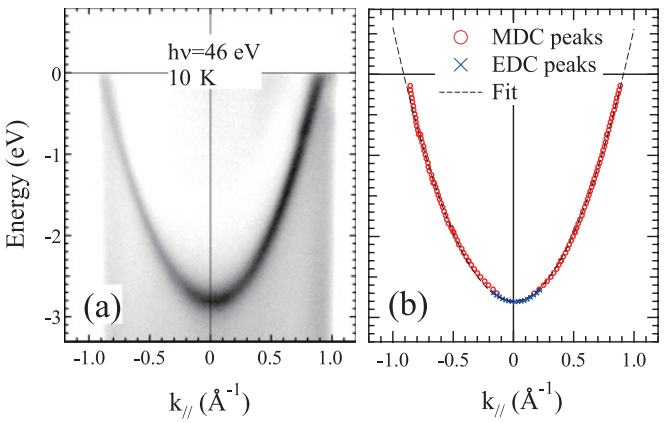

FIG. 2. (Color online) (a) The ARPES intensity plot of the Al(100) surface state in a wide energy range, taken at $h\nu = 46$ eV and 10 K. (b) The band points obtained by the MDC and EDC line shape analyses. The dashed line shows a fit to a parabolic function.

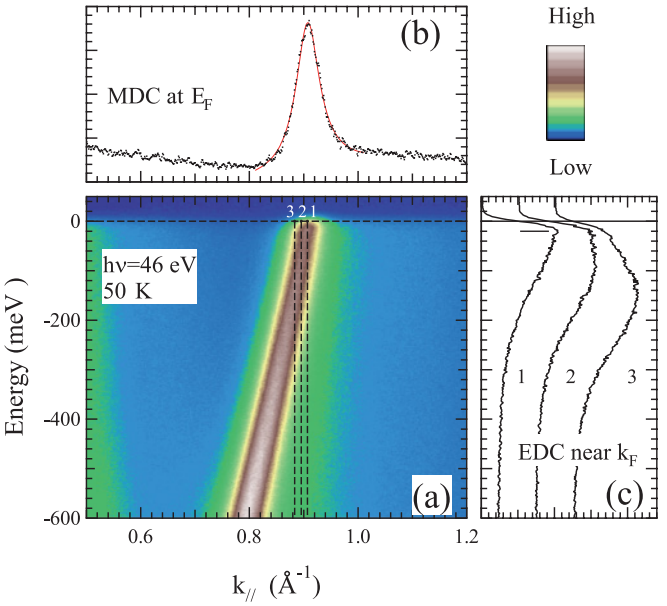

FIG. 3. (Color online) (a) The ARPES intensity plot of the Al(100) surface state near E_F, taken at $h\nu = 46$ eV and 50 K. (b) The MDC at E_F. (c) The EDCs along the dashed lines 1,2,3 in (a).

surface carrier density n is given by $n = k_F^2/2\pi = (1.3 \pm 0.1) \times 10^{15}$ electrons/cm^2. The density of states at E_F for the unit volume was calculated as $\rho_0 = m_b/\pi\hbar^2 = (4.7 \pm 0.1) \times 10^{-2}$ states/(eV Å^2).

Figure 3(a) shows the high-resolution ARPES intensity plot of the Al(100) surface state near E_F taken at $h\nu = 46$ eV and at $T = 50$ K along the $\overline{\Gamma X}$. To quantitatively analyze the spectral shape, we used a Lorentzian on a linear background to fit the MDCs, as shown in Fig. 3(b).[46] We obtained the peak position and MDC linewidth (δk) as functions of ω.

Figure 3(c) shows three EDCs (1,2,3) obtained from cuts along the broken lines in Fig. 3(a). Figure 3(c) shows that the spectral width becomes narrower as the peak approaches E_F. In cut 1, a narrow peak near E_F and a hump structure can be recognized. We will examine the EDC spectral feature in more detail in Sec. IV E.

B. Linewidth and relaxation time due to the electron-defect interaction

By fitting the observed MDC at E_F and at $h\nu = 46$ eV to a Lorentzian [Solid line in Fig. 3(b)], the width was determined to be (0.042 ± 0.001) Å^{-1}. By subtracting the contribution from the angular resolution ($\Delta k = 0.017$ Å^{-1}), we estimated the intrinsic linewidth broadening at E_F to be $\delta k = 0.038$ Å^{-1}. Note that the linewidth broadening due to the final-state broadening is negligible for the surface states,[14,47,48] and the lifetime broadening due to the electron-phonon and electron-electron interactions is ~ 0 at low temperature at E_F. As we have carefully checked the cleanliness of the sample surface, impurities, such as adsorbed molecules or extrinsic elements in Al, were unlikely to have been the main source of the energy-independent term. Therefore, the lifetime broadening at low temperature at E_F should have derived from the electron-defect interactions, $\Gamma_0 = 2|\mathrm{Im}\Sigma_{ed}|$.

The full width at half maximum (FWHM) of the linewidth ($2\eta = 2|\mathrm{Im}\Sigma_{ed}|$) was calculated from

$$2\eta = 2\omega_0^* \left[\left(1 + \frac{\delta k}{2k_F} \right)^2 - 1 \right] \quad (5)$$

(see Appendix A). Using $\omega_0^* = 2.81$ eV, $k_F = 0.907$ Å^{-1}, and $\delta k = 0.038$ Å^{-1}, the linewidth at E_F is calculated as $\Gamma_0 = 2\eta = (0.238 \pm 0.006)$ eV, indicating $\eta = |\mathrm{Im}\Sigma_0| = (0.119 \pm 0.003)$ eV. The measured EDC linewidth at the $\overline{\Gamma}$ point at 10 K was $\Gamma_{tot} = 0.284$ eV. The contribution from $\Gamma_{ep} + \Gamma_{ee}$ is given by $\Gamma_{tot} - \Gamma_0 = 0.046$ eV (46 meV).

Although the linewidth at $\overline{\Gamma}$ is comparable to the narrowest one reported to date, we could not improve the linewidth by repeated cycles of annealing and sputtering. It suggests that a complete removal of these defects by conventional cleaning methods may not be simple. The electrons at the surface are strongly scattered by surface defects.

The mean distance $\bar{l}$ between defects may be evaluated by the inverse of the MDC width, $\bar{l} = 1/\delta k = (26 \pm 1)$ Å. Therefore, the density of the lattice defects is estimated by $n_i = 1/\bar{l}^2 = (1.5 \pm 0.1) \times 10^{13}$ /cm^2.

We also attempted to evaluate some of the parameters that characterize the transport properties of the surface electronic state. We can evaluate the relaxation time via $\tau = \frac{\hbar}{2|\mathrm{Im}\Sigma_0|} = (2.8 \pm 0.1) \times 10^{-15}$ s at low temperature. The mobility can be calculated as $\mu = e\tau/m_b = (4.4 \pm 0.2)$ cm^2/(V s), and the sheet conductivity is $\sigma = ne^2\tau/m_b = (9.1 \pm 0.3) \times 10^{-4}$ S/□. The mobility is much smaller than that of the high-mobility two-dimensional electron gas, which is mainly due to the high density of defects at the surface.

The potential energy of the defect can be evaluated using $\frac{\hbar}{\tau} = 2|\mathrm{Im}\Sigma_0| = 2\pi n_i \rho_0 U_0^2$,[51] where U_0 is the Fourier component of the potential energy with $q = 0$. Using the parameters we evaluated, we obtained $U_0 = \sqrt{\frac{|\mathrm{Im}\Sigma_0|}{\pi n_i \rho_0}} = (23 \pm 2)$ eV Å^2. The magnitude of the potential energy of the defect, therefore, was evaluated as $V_d \sim U_0/\bar{l}^2 = (0.034 \pm 0.003)$ eV. Since the magnitude of the potential is much smaller than the Fermi energy, $V_d/\omega_0^* \sim 0.01$, it is reasonable to assume that the electron-defect scattering at E_F is elastic.

C. Evaluation of the electron-phonon and electron-electron coupling parameters

Figure 4 clearly shows a kink structure in the energy-band dispersion at ∼−40 meV. Note that the surface and bulk Debye temperatures of Al are 573 K ($k_B\Theta_D = 49$ meV) (Ref. 30) and 426 K ($k_B\Theta_D = 37$ meV) (Ref. 49), respectively. Because the energy of the kink agrees well with the energy scale of the Debye temperature of Al, it is reasonable to assume that the kink at ∼−40 meV is derived from the electron-phonon interaction.[1,3]

Recently, Sklyadneva *et al.* have reported an *ab initio* study of the electron-phonon interaction in the Al(100) surface state that was based on density-functional theory and that used a linear response approach for the plane-wave pseudopotential representation.[41] The calculated electron-phonon spectral function, or the Eliashberg function [$\alpha^2F(\omega)$], has a cutoff energy of ∼43 meV, which is consistent with the kink energy

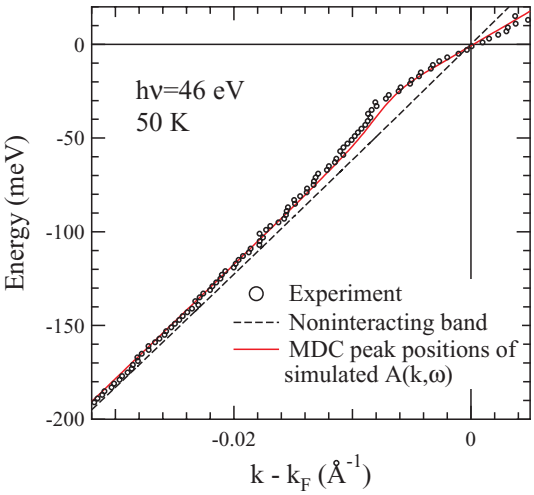

FIG. 4. (Color online) The circles represent the band points near E_F, as determined by the MDC analysis. The dashed line indicates the parabolic function determined in Fig. 2(b), which was assumed to be the noninteracting band for the evaluation of $\mathrm{Re}\Sigma_{ep}$. The solid line indicates the MDC peak positions of the simulated $A(k,\omega)$.

in Fig. 4. Because the theoretical Eliashberg function depends on the k position,[40,41] the Eliashberg function at E_F should be used for quantitative analyses. Although Eiguren *et al.* (Ref. 40) calculated the Eliashberg function averaged over the Fermi level, this approach may be limited.[31,41] We therefore used the more recent theoretical calculation of α^2F at the $\overline{\Gamma}$ point described by Sklyadneva *et al.*[41] As described in Sec. IV D, the magnitude of the theoretical α^2F (solid line in the inset of Fig. 6 below) seems to be slightly smaller. Therefore, we multiplied by a factor of 1.15 to obtain the theoretical self-energies (dashed line in the inset of Fig. 6).

The lifetime broadening due to the electron-phonon interaction is given by

$$\begin{aligned}\Gamma_{ep}(\omega,T) &= 2|\mathrm{Im}\Sigma_{ep}(\omega,T)| \\ &= 2\pi \int_0^\infty \alpha^2F(\nu)[2n(\nu,T) \\ &\quad + f(\nu+\omega,T) + f(\nu-\omega,T)]d\nu, \end{aligned} \quad (6)$$

where $n(\nu,T)$ and $f(\nu,T)$ are the Bose-Einstein and Fermi-Dirac distribution functions, respectively.[20] Based on the Kramers-Kronig transform, as given by Eq. (4), we calculated the theoretical $\mathrm{Re}\Sigma_{ep}$ using the theoretical $\mathrm{Im}\Sigma_{ep}$.

Figures 5(a1) and 5(b1) show the experimentally evaluated $\mathrm{Re}\Sigma_{ep}$ at 10 K and 50 K, respectively. The dashed lines in Figs. 5(a1) and 5(b1) show the gradient of the experimental $\mathrm{Re}\Sigma_{ep}$ at E_F, giving the electron-phonon coupling parameter λ_{ep}. Using the gradient of the observed $\mathrm{Re}\Sigma_{ep}$ at E_F [dashed line in Fig. 5(b1)], the parameter was determined to be $\lambda_{ep} = 0.67 \pm 0.05$ at 50 K. The solid lines in Figs. 5(a1) and 5(b1) indicate that the theoretical $\mathrm{Re}\Sigma_{ep}$ agrees with the experimental $\mathrm{Re}\Sigma_{ep}$. These results confirm that the kink structure originates from the electron-phonon interaction.

Figures 5(a2) and 5(b2) show the experimentally evaluated $2|\mathrm{Im}\Sigma| - \Gamma_0$ at 10 and 50 K, respectively. Here Γ_0 represents the lifetime broadening due to the electron-defect interaction. The solid lines in Figs. 5(a2) and 5(b2) show the theoretical

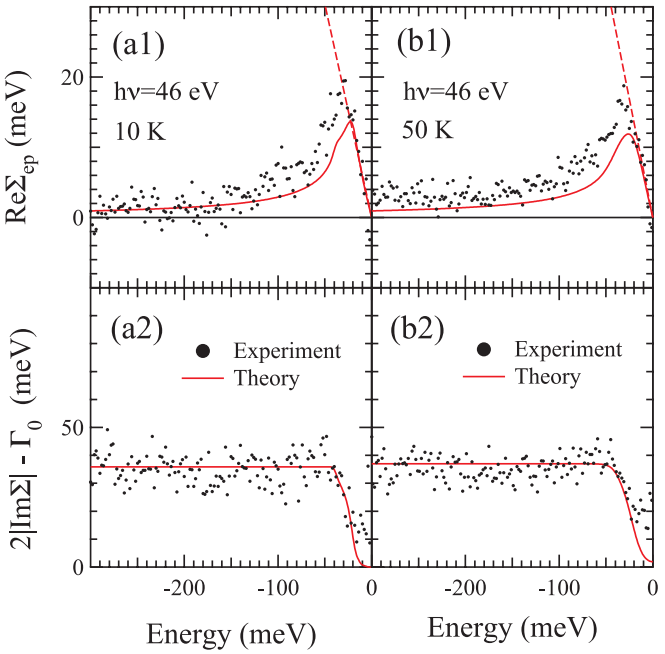

FIG. 5. (Color online) (a1) and (b1) indicate the experimentally obtained $\mathrm{Re}\Sigma_{ep}$ (the filled circles) at 10 and 50 K, respectively. The dashed lines indicate the gradient at E_F. The solid lines represent the theoretical $\mathrm{Re}\Sigma_{ep}$. (a2) and (b2) indicate the experimentally obtained $2|\mathrm{Im}\Sigma| - \Gamma_0$ (the filled circles) at 10 and 50 K, respectively. The solid lines represent the theoretical $2|\mathrm{Im}\Sigma_{ep}|$.

$\Gamma_{ep} = 2|\mathrm{Im}\Sigma_{ep}|$, which explains the decrease in the observed linewidth above ~40 meV.

The linewidth due to the electron-phonon interaction at 10–50 K is $\Gamma_{ep} \sim 0.036$ eV for $\omega < -k_B\Theta_D$. Therefore, the linewidth broadening due to the electron-electron interaction should be $\Gamma_{ee} = \Gamma_{tot} - \Gamma_0 - \Gamma_{ep} \sim 0.010$ eV at $\omega_0^* = -2.81$ eV. For the two-dimensional Fermi liquid, the lifetime broadening due to the electron-electron interaction is given by $2|\mathrm{Im}\Sigma_{ee}(\omega)| = 2\beta\omega^2[1/4 + \ln 2 - (1/2)\ln|\omega/\omega_0|]$.[50] At the bottom of the energy band, we assumed that $2|\mathrm{Im}\Sigma_{ee}(\omega_0^*)| = 2\beta^*\omega_0^{*2}[1/4 + \ln 2] \sim 0.010$ eV. The β^* coefficient was determined to be 0.0007 eV^{-1}, which is much smaller than that obtained for the strongly correlated Ni(111) surface state ($\beta^* \sim 1.5$ eV^{-1}).[20] Based on the relation $\lambda_{ee} = \beta^*\omega_0^*\zeta$ ($\zeta \sim 1.5$) (Appendix B), the coupling parameter due to the electron-electron interaction was estimated to be $\lambda_{ee} \sim 0.003$, which is much smaller than $\lambda_{ep} = 0.67$. Thus the renormalization due to the electron-electron interaction is negligible for the Al(100) surface state.

The effective mass enhancement of the Al(100) surface state at E_F can be evaluated as $m^*/m_b = 1 + \lambda_{ep} + \lambda_{ee} \sim 1.7$. The effective mass enhancement is mainly derived from the electron-phonon interaction.

D. Evaluation of $\lambda_{ep}(T)$

Because the Fermi-Dirac and Bose-Einstein functions in Eq. (6) are temperature dependent, the linewidth ($2|\mathrm{Im}\Sigma_{ep}|$) is also temperature dependent. As $\mathrm{Re}\Sigma_{ep}$ is related to $\mathrm{Im}\Sigma_{ep}$ via the Kramers-Kronig transform, $\lambda_{ep}(T)$ [as determined by Eq. (2)] should be temperature dependent. The magnitude of

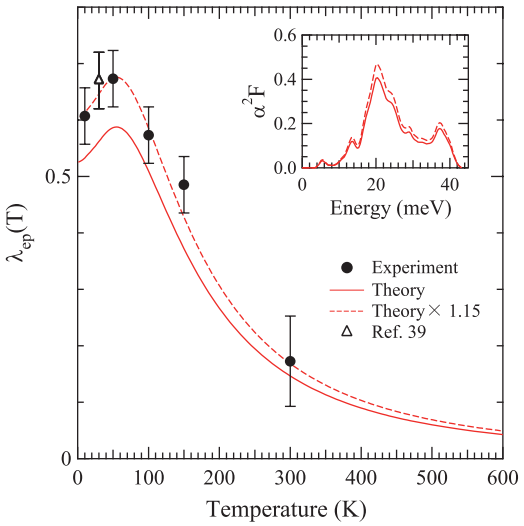

FIG. 6. (Color online) The temperature dependence of the experimental λ_{ep} compared to the theoretical calculations.

$\lambda_{ep}(T)$ should give a measure of the temperature dependence of the kink structure due to the electron-phonon interaction. Figure 6 shows $\lambda_{ep}(T)$ determined at $T = 10, 50, 100, 150, 300$ K. With increasing temperature, the $\lambda_{ep}(T)$ is at first slightly enhanced. It reaches its maximum at approximately 50 K, $\lambda_{ep} = 0.67$, and then decreases rapidly above 100 K. It indicates that the kink structure vanishes rapidly at elevated temperatures.

According to the analytical calculation, the temperature dependence of the electron-phonon coupling parameter is described by

$$\lambda_{ep}(T) = -\left.\frac{\partial \mathrm{Re}\Sigma_{ep}(\omega,T)}{\partial\omega}\right|_{\omega=0} = 2\int_0^{\hbar\omega_{max}} \frac{\alpha^2F(\nu)}{\nu} G\left(\frac{\nu}{k_BT}\right) d\nu, \quad (7)$$

where

$$G(1/t) = 4\left(\frac{1}{\pi t}\right)^2 \sum_{n=0}^{\infty} \frac{2n+1}{\left[(2n+1)^2 + \left(\frac{1}{\pi t}\right)^2\right]^2} \quad (8)$$

and $t = \frac{k_BT}{\nu}$.[29] Assuming that the Eliashberg function α^2F is not temperature dependent, $\lambda_{ep}(T)$ can be calculated based on Eqs. (7) and (8).

Using the Eliashberg function as given by Sklyadneva *et al.*,[41] we calculated the coupling parameter at $T = 0$ K and obtained $\lambda_{ep} = 0.526$, which agrees well with the 0.51 ± 0.01 explicitly given in Ref. 41. The experimentally evaluated λ_{ep} value at 10 K was 0.61, which is slightly larger than the theoretical one. The theoretical λ_{ep} has been reported to increase from $\overline{\Gamma}$ toward E_F.[40,41] Since we used the Eliashberg function at the $\overline{\Gamma}$ point in this study, the coupling strength may have been underestimated. We therefore multiplied the theoretical Eliashberg function by a factor of 1.15 (the dashed line in the inset of Fig. 6) to reproduce the experimental value (the dashed line in Fig. 6), and this explained $\lambda_{ep}(T)$ reasonably well for the entire temperature range.

It should be noted that temperature-induced defects do not affect the magnitude of the electron-phonon coupling

parameter. Because $\Gamma_0(T) = 2|\mathrm{Im}\Sigma_0(T)|$ is assumed to be energy independent, the Kramers-Kronig transform of $\mathrm{Im}\Sigma_0(T)$ should give $\mathrm{Re}\Sigma_0(T) = 0$, and the temperature-induced defects should not affect the magnitude of the kink structure. This independence explains why the coupling parameter, λ_{ep}, given by Eq. (2) is not affected by the temperature-induced defects.

E. Quasiparticle peak near E_F

Although a narrow EDC peak structure near E_F can be discerned, the quasiparticle intensity is not significant, and the spectral feature is further obscured by the Fermi cutoff. For the detailed analyses, we normalized and symmetrized the spectral intensities at 50 K to remove the Fermi cutoff effect. The symmetrized EDCs in Fig. 7 clearly show the quasiparticle peak near E_F. The observed spectral features are similar to those for the Be(0001) surface state[22,23] in that the electron-phonon interaction yields a peak-hump structure in the EDCs.

To further confirm the origin of the quasiparticle peak, we simulated the spectral function $A(k,\omega)$, including the self-energy due to the electron-defect and electron-phonon interactions obtained in this study. We assumed the self-energy to be $\mathrm{Re}\Sigma = \mathrm{Re}\Sigma_{ep}$, $\mathrm{Im}\Sigma = \mathrm{Im}\Sigma_{ep} + \mathrm{Im}\Sigma_0$, and $\mathrm{Im}\Sigma_0 = -0.119$ eV. The contribution from the electron-electron interaction was negligible in this energy range. Figure 7 shows the simulated EDCs (solid lines), which reproduce the observed EDCs. They confirm that the narrow peak originates from the electron-phonon interaction.

Figure 8 shows the EDC peak positions obtained from experiments and those given by the simulated spectral function. The experimental EDC peaks were determined by the fit of the experimental EDC to the two Lorentzians. The theoretical peak positions were determined by searching for the minima in the second derivatives of the calculated EDCs. Note that the EDCs are split into two peaks due to the self-energy correction within the Debye energy ($|\omega| < k_B\Theta_D$). Peak A in the EDC crosses E_F and becomes less dispersive as the peak gets closer to -25 meV, where the theoretical Eliashberg function has a peak. By contrast,

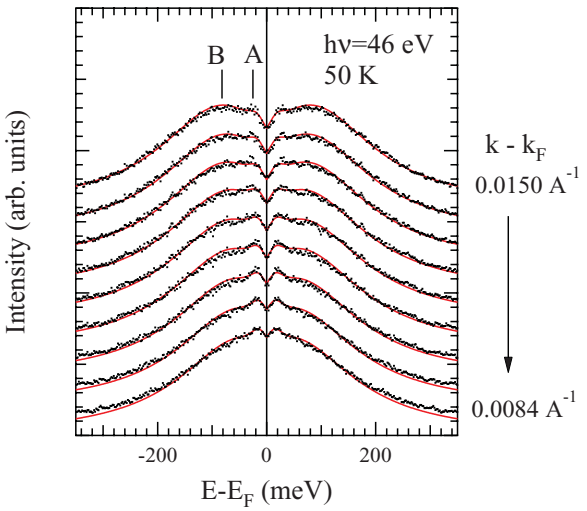

FIG. 7. (Color online) The symmetrized experimental EDCs (the filled circles) compared to the calculated EDCs (the solid lines).

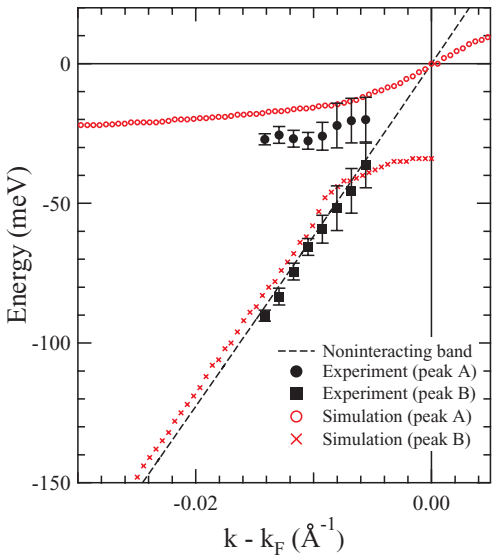

FIG. 8. (Color online) The experimental symmetrized EDC peaks compared to those given by the simulated $A(k,\omega)$. The dashed line indicates the parabolic function determined in Fig. 2(b), which was assumed to be the noninteracting band in the evaluation of $\mathrm{Re}\Sigma_{ep}$.

the EDC peak B does not cross E_F and agrees with the noninteracting band dispersion for the lower-energy region.

The dispersional width of peak A is rather narrow, $\sim$25 meV, which explains the narrower EDC linewidth compared to the dispersive peak B. The width of peak A is probably limited by the energy resolution ($\Delta E = 15$ meV).

The MDC peak positions of the simulated $A(k,\omega)$ also correspond well to the experimental MDC peak positions in Fig. 4.

V. CONCLUSIONS

We performed a high-resolution ARPES study of the surface-derived state of Al(100) to evaluate the coupling parameters of many-body interactions. We were able to fit the observed band dispersion of the surface state using a parabolic function with a Fermi energy of $\omega_0^* = 2.81 \pm 0.03$ eV and a Fermi wave vector of $k_F = 0.907 \pm 0.005$ Å^{-1}. Based on the MDC linewidth at E_F, we found a significant contribution from the electron-defect interaction ($\Gamma_0 = 0.238$ eV). A kink structure derived from the electron-phonon interaction existed in the energy-band dispersion at ~ -40 meV. The electron-phonon and electron-electron coupling parameters at 50 K were determined to be $\lambda_{ep} = 0.67 \pm 0.05$ and $\lambda_{ee} \sim 0.003$, respectively. The effective mass enhancement of the Al(100) surface state was mainly derived from the electron-phonon interaction. The electron-phonon coupling parameter at the surface was 50% larger than the bulk value. We studied the temperature dependence of the kink structure, as measured by $\lambda_{ep}(T)$, and found it to be explained well by a theoretical calculation based on the Eliashberg function. A quasiparticle peak with a narrow linewidth (15–20 meV) was observed near E_F, and the EDC spectra were quantitatively explained by the simulated spectral function incorporating the self-energy evaluated in this study.

We showed that the electron-phonon coupling parameter for the surface state is approximately 50% larger than that

for the bulk state [$\lambda_{ep} = 0.43$ (Ref. 6)]. The band-structure calculation for Al thin films suggests that the electron-phonon coupling parameter can be larger than the bulk value and can oscillate depending on the thickness of the film.[52] In a future study, it would be interesting to see the layer dependence of the coupling parameter as it relates to the superconducting transition temperature. As the ARPES technique is making rapid progress, we believe we will be able to observe the superconducting transition in Al by high-resolution ARPES in the future.

ACKNOWLEDGMENTS

This work was partially supported by a Grant-in-Aid for Scientific Research (No. 22340103) by MEXT of Japan. We thank the N-BARD, Hiroshima University for supplying the liquid helium. The synchrotron radiation experiments were performed with the approval of HSRC (Proposals No. 07-A-41 and 10-A-49). We thank D. Hirayama and T. Habuchi for their technical support with the synchrotron radiation measurements.

APPENDIX A

We describe here the linewidth due to the electron-impurity interaction. Note that this description is also applicable to the electron-defect interaction. The single-particle Green's function due to the electron-impurity interaction is given by[51]

$$G(k,\omega) = \frac{1}{\omega - \omega_k + i\eta}, \tag{A1}$$

where $\eta = -\mathrm{Im}\Sigma_{ei}(\omega) = \hbar/\tau > 0$ is the half width at half maximum of the peak and τ is the relaxation time. The spectral function is given by

$$A(k,\omega) = -\frac{1}{\pi}\mathrm{Im}G(k,\omega) = \frac{1}{\pi}\frac{\eta}{(\omega-\omega_k)^2+\eta^2}. \tag{A2}$$

At the fixed point k, plotting $A(k,\omega)$ as a function of ω creates an EDC curve, which is a Lorentzian with a linewidth of $2\eta = 2|\mathrm{Im}\Sigma_{ei}|$.

To determine the MDC line shape, we assume that the noninteracting band is parabolic of the form $\omega_k = -\omega_0 + (\omega_0/k_F^2)k^2$. The spectral function is calculated by

$$A(k,\omega) = \frac{1}{\pi}\frac{k_F^2}{\omega_0}\frac{\frac{k_F^2\eta}{\omega_0}}{\left[k^2 - k_F^2\left(1+\frac{\omega}{\omega_0}\right)\right]^2 + \left(\frac{k_F^2\eta}{\omega_0}\right)^2}. \tag{A3}$$

Fixing the energy ($\omega = \mathrm{const}$), $A(k,\omega)$ as a function of k gives the MDC line shape. Note that this expression is not a Lorentzian. Solution of the equation $A(k_{\max},\omega) = \frac{1}{2}A(k_{\max} + \delta k/2,\omega)$, where $k_{\max}$ is the wave number giving the maximum intensity at a given ω and δk is the FWHM of the MDC linewidth, yields

$$\delta k = 2k_F\left(\sqrt{1+\frac{\eta}{\omega_0}+\frac{\omega}{\omega_0}} - \sqrt{1+\frac{\omega}{\omega_0}}\right). \tag{A4}$$

Based on Eq. (A4), the MDC width at $\omega = 0$ (E_F) is given by

$$\delta k = 2k_F\left(\sqrt{1+\frac{\eta}{\omega_0}} - 1\right).$$

Therefore, the linewidth (FWHM) due to the electron-defect interaction is

$$2\eta = 2\omega_0\left[\left(1+\frac{\delta k}{2k_F}\right)^2 - 1\right]. \tag{A5}$$

Near E_F ($k \sim k_F$ and $\omega \sim 0$), we have the approximation

$$\begin{aligned}&\left[k^2 - k_F^2\left(1+\frac{\omega}{\omega_0}\right)\right]^2 \\ &= \left(k - k_F\sqrt{1+\frac{\omega}{\omega_0}}\right)^2\left(k + k_F\sqrt{1+\frac{\omega}{\omega_0}}\right)^2 \\ &\sim \left(k - k_F - \frac{k_F\omega}{2\omega_0}\right)^2(2k_F)^2.\end{aligned}$$

Note that this approximation is essentially the same as that involving adopting a linear function as a noninteracting band near E_F.[4] The MDC line shape near E_F is then approximated by

$$A(k,\omega) \sim \frac{1}{\pi}\frac{k_F}{2\omega_0}\frac{\frac{k_F\eta}{2\omega_0}}{\left(k - k_F - \frac{k_F\omega}{2\omega_0}\right)^2 + \left(\frac{k_F\eta}{2\omega_0}\right)^2}, \tag{A6}$$

which is a Lorentzian with a width of $\frac{k_F\eta}{\omega_0}$.

In the case of $\eta/\omega_0 \ll 1$ and at $\omega \sim 0$, Eq. (A4) also gives the MDC width as

$$\delta k \sim 2k_F\left[\left(1+\frac{\eta}{2\omega_0}+\frac{\omega}{2\omega_0}\right) - \left(1+\frac{\omega}{2\omega_0}\right)\right] = \frac{k_F\eta}{\omega_0}. \tag{A7}$$

APPENDIX B

Here we develop an expression for the two-dimensional Fermi liquid, $\lambda_{ee} = \beta^*\omega_0^*\zeta$, where λ_{ee} is the coupling parameter due to the electron-electron interaction, β^* is the coefficient in the observed $2|\mathrm{Im}\Sigma_{ee}(\omega)|$, and $-\omega_0^*$ is the lowest energy for the observed parabolic band.

The imaginary part of the self-energy for the two-dimensional Fermi liquid was estimated to be $2|\mathrm{Im}\Sigma_{ee}(\omega)| = 2\beta\omega^2[1/4 + \ln 2 - (1/2)\ln|\omega/\omega_0|]$ for $|\omega| < \omega_0$, where $-\omega_0$ is the lowest energy of the noninteracting band.[50] Because $2|\mathrm{Im}\Sigma_{ee}(\omega)|$ is divergent for $\omega \to \pm\infty$, we assumed $2|\mathrm{Im}\Sigma_{ee}(\omega)| = 2|\mathrm{Im}\Sigma_{ee}(\omega_0)|$ for $|\omega| > \omega_0$ and electron-hole symmetry for the analytical calculation.

Based on the Kramers-Kronig transform, the coupling parameter is given by

$$\begin{aligned}\lambda_{ee} &= -\left.\frac{\partial\mathrm{Re}\Sigma_{ee}}{\partial\omega}\right|_{\omega=0} = -\frac{1}{\pi}\mathrm{P}\int_{-\infty}^{+\infty}\frac{\mathrm{Im}\Sigma_{ee}(\omega')}{\omega'^2}d\omega' \\ &= -\frac{1}{\pi}P\int_{-\infty}^{-\omega_0}\frac{\mathrm{Im}\Sigma_{ee}(\omega_0)}{\omega'^2}d\omega' - \frac{1}{\pi}\mathrm{P}\int_{-\omega_0}^{+\omega_0}\frac{\mathrm{Im}\Sigma_{ee}(\omega)}{\omega'^2}d\omega' \\ &\quad - \frac{1}{\pi}\mathrm{P}\int_{+\omega_0}^{+\infty}\frac{\mathrm{Im}\Sigma_{ee}(\omega_0)}{\omega'^2}d\omega' \\ &= \beta\omega_0\frac{2}{\pi}\left[\frac{3}{4}+\ln 2\right] + \frac{\beta\omega_0^2}{\pi}\left[\frac{1}{4}+\ln 2\right]\times 2\int_{+\omega_0}^{+\infty}\frac{1}{\omega'^2}d\omega' \\ &= \beta\omega_0\times\frac{4}{\pi}\left[\frac{1}{2}+\ln 2\right] = \beta\omega_0\zeta,\end{aligned}$$

$$\zeta \equiv \frac{4}{\pi}\left[\frac{1}{2}+\ln 2\right] \approx 1.519. \tag{B1}$$

The observed β^* and ω_0^* are related to β and ω_0 by $\beta^* = \beta(1+\lambda_{ee})$ and $\omega_0^* = \omega_0/(1+\lambda_{ee})$.[4] Therefore, the product $\beta\omega_0$ is conserved: $\beta\omega_0 = \beta^*\omega_0^*$. Finally we have the relation $\lambda_{ee} = \beta^*\omega_0^*\zeta$.

*Corresponding author: kshimada@hiroshima-u.ac.jp

[1] T. Valla, A. V. Fedorov, P. D. Johnson, and S. L. Hulbert, Phys. Rev. Lett. **83**, 2085 (1999).

[2] *Very High Resolution Photoelectron Spectroscopy*, edited by S. Hüfner, Lecture Notes in Physics Vol. 715 (Springer-Verlag, Berlin, 2007).

[3] M. Higashiguchi, K. Shimada, K. Nishiura, X. Y. Cui, H. Namatame, and M. Taniguchi, Phys. Rev. B **72**, 214438 (2005).

[4] X. Y. Cui, K. Shimada, Y. Sakisaka, H. Kato, M. Hoesch, T. Oguchi, Y. Aiura, H. Namatame, and M. Taniguchi, Phys. Rev. B **82**, 195132 (2010).

[5] W. L. McMillan, Phys. Rev. **167**, 331 (1968).

[6] J. P. Carbotte, Rev. Mod. Phys. **62**, 1027 (1990).

[7] W. A. Harrison, Phys. Rev. **116**, 555 (1959).

[8] C. O. Larson and W. L. Gordon, Phys. Rev. **156**, 703 (1967).

[9] H. J. Levinson, F. Greuter, and E. W. Plummer, Phys. Rev. B **27**, 727 (1983).

[10] J. Bardeen, L. N. Cooper, and J. R. Schrieffer, Phys. Rev. **108**, 1175 (1957).

[11] E. Caruthers, L. Kleinman, and G. P. Alldredge, Phys. Rev. B **8**, 4570 (1973).

[12] G. V. Hansson and S. A. Flodström, Phys. Rev. B **18**, 1562 (1978).

[13] M. Seel, Phys. Rev. B **28**, 778 (1983).

[14] S. D. Kevan, N. G. Stoffel, and N. V. Smith, Phys. Rev. B **31**, 1788 (1985).

[15] W. Hummel and H. Bross, Phys. Rev. B **58**, 1620 (1998).

[16] Ph. Hofmann, Ch. Sondergaard, S. Agergaard, S. V. Hoffmann, J. E. Gayone, G. Zampieri, S. Lizzit, and A. Baraldi, Phys. Rev. B **66**, 245422 (2002).

[17] G. Nicolay, F. Reinert, S. Schmidt, D. Ehm, P. Steiner, and S. Hüfner, Phys. Rev. B **62**, 1631 (2000).

[18] F. Reinert, G. Nicolay, S. Schmidt, D. Ehm, and S. Hüfner, Phys. Rev. B **63**, 115415 (2001).

[19] J. Kutzner, R. Paucksch, C. Jabs, H. Zacharias, and J. Braun, Phys. Rev. B **56**, 16003 (1997).

[20] M. Higashiguchi, K. Shimada, M. Arita, Y. Miura, N. Tobita, X. Y. Cui, Y. Aiura, H. Namatame, and M. Taniguchi, Surf. Sci. **601**, 4005 (2007).

[21] Y. Nishimura, M. Kakeya, M. Higashiguchi, A. Kimura, M. Taniguchi, H. Narita, Y. Cui, M. Nakatake, K. Shimada, and H. Namatame, Phys. Rev. B **79**, 245402 (2009).

[22] M. Hengsberger, R. Frésard, D. Purdie, P. Segovia, and Y. Baer, Phys. Rev. B **60**, 10796 (1999).

[23] S. LaShell, E. Jensen, and T. Balasubramanian, Phys. Rev. B **61**, 2371 (2000).

[24] A. Ishii and T. Aisaka, Surf. Sci. **242**, 250 (1991).

[25] S. K. Ma and Kenneth W.-K. Shung, Phys. Rev. B **49**, 10617 (1994).

[26] E. E. Krasovskii and W. Schattke, Phys. Rev. Lett. **93**, 027601 (2004).

[27] A. Damascelli, Z. Hussain, and Z. X. Shen, Rev. Mod. Phys. **75**, 473 (2003).

[28] J. E. Gayone, C. Kirkegaard, J. W. Wells, S. V. Hoffmann, Z. Li, and P. Hofmann, Appl. Phys. A **80**, 943 (2005).

[29] G. Grimvall, *The Electron-Phonon Interaction in Metals* (North-Holland, Amsterdam, 1981).

[30] M. Fuglsang Jensen, T. K. Kim, S. Bengió, I. Yu. Sklyadneva, A. Leonardo, S. V. Eremeev, E. V. Chulkov, and Ph. Hofmann, Phys. Rev. B **75**, 153404 (2007).

[31] I. Y. Sklyadneva, R. Heid, V. M. Silkin, A. Melzer, K. P. Bohnen, P. M. Echenique, T. Fauster, and E. V. Chulkov, Phys. Rev. B **80**, 045429 (2009).

[32] S. V. Eremeev and E. V. Chulkov, Phys. Solid State **51**, 854 (2009).

[33] S. V. Eremeev, S. S. Tsirkin, and E. V. Chulkov, Phys. Rev. B **82**, 035424 (2010).

[34] S. LaShell, B. A. McDougall, and E. Jensen, Phys. Rev. B **74**, 033410 (2006).

[35] B. A. McDougall, T. Balasubramanian, and E. Jensen, Phys. Rev. B **51**, 13891 (1995).

[36] R. Matzdorf, G. Meister, and A. Goldmann, Phys. Rev. B **54**, 14807 (1996).

[37] A. Eiguren, B. Hellsing, F. Reinert, G. Nicolay, E. V. Chulkov, V. M. Silkin, S. Hüfner, and P. M. Echenique, Phys. Rev. Lett. **88**, 066805 (2002).

[38] F. Reinert, B. Eltner, G. Nicolay, F. Forster, S. Schmidt, and S. Hüfner, Physica B **351**, 229 (2004).

[39] J. Jiang, M. Higashiguchi, N. Tobida, K. Tanaka, S. Fukuda, H. Hayashi, K. Shimada, H. Namatame, and M. Taniguchi, J. Surf. Sci. Nanotechnology **7**, 57 (2009).

[40] A. Eiguren, B. Hellsing, E. V. Chulkov, and P. M. Echenique, Phys. Rev. B **67**, 235423 (2003).

[41] I. Y. Sklyadneva, E. V. Chulkov, and P. M. Echenique, J. Phys.: Condens. Matter **20**, 165203 (2008).

[42] K. Shimada, M. Arita, Y. Takeda, H. Fujino, K. Kobayashi, T. Narimura, H. Namatame, and M. Taniguchi, Surf. Rev. Lett. **9**, 529 (2002).

[43] Y. Aiura, H. Bando, T. Miyamoto, A. Chiba, R. Kitagawa, S. Maruyama, and Y. Nishihara, Rev. Sci. Instrum. **74**, 3177 (2003).

[44] S. Hüfner, *Photoelectron Spectroscopy Principles and Applications*, 3rd ed. (Springer-Verlag, Berlin, 2003).

[45] E. E. Krasovskii, W. Schattke, P. Jiříček, M. Vondráček, O. V. Krasovska, V. N. Antonov, A. P. Shpak, and I. Bartoš, Phys. Rev. B **78**, 165406 (2008).

[46] In Fig. 3(b), the background of the MDC is not constant. We assume that this is mainly derived from the k_z broadening effect of the bulk-derived states (Refs. 44,47,48). We fitted the observed MDC to an asymmetric Lorentzian (Ref. 53), and found that the asymmetry was negligible. By restricting the fitting $k_\parallel$ range to $\sim$0.2 Å^{-1}, the MDC line shape can be well represented by a symmetric Lorentzian on a linear background.

[47] N. V. Smith, P. Thiry, and Y. Petroff, Phys. Rev. B **47**, 15476 (1993).

[48] T.-C. Chiang, Chem. Phys. **251**, 133 (2000).

[49] C. Kittel, *Introduction to Solid State Physics*, 6th ed. (Wiley, New York, 1986).

[50] C. Hodges, H. Smith, and J. W. Wilkins, Phys. Rev. B **4**, 302 (1971).

[51] S. Doniach and E. H. Sondheimer, *Green's Functions for Solid State Physicists* (Addison-Wesley, Redwood City, CA, 1974).

[52] G. Q. Huang, Phys. Rev. B **78**, 214514 (2008).

[53] S. Doniach and M. Sunjic, J. Phys. C **3**, 285 (1978).